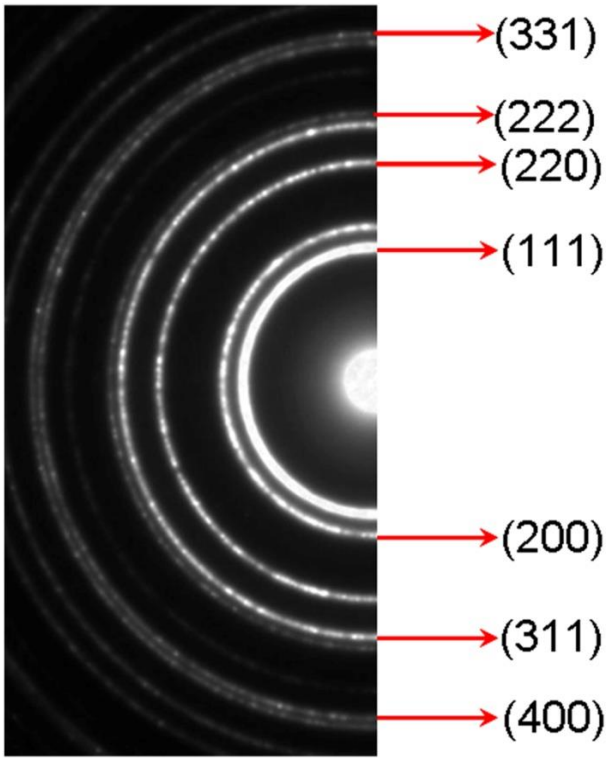

Supplementary Figure 1. The selected area diffraction patterns of the Pt thin film. The diffraction pattern can be well indexed with the Face-Centered Cubic Pt.

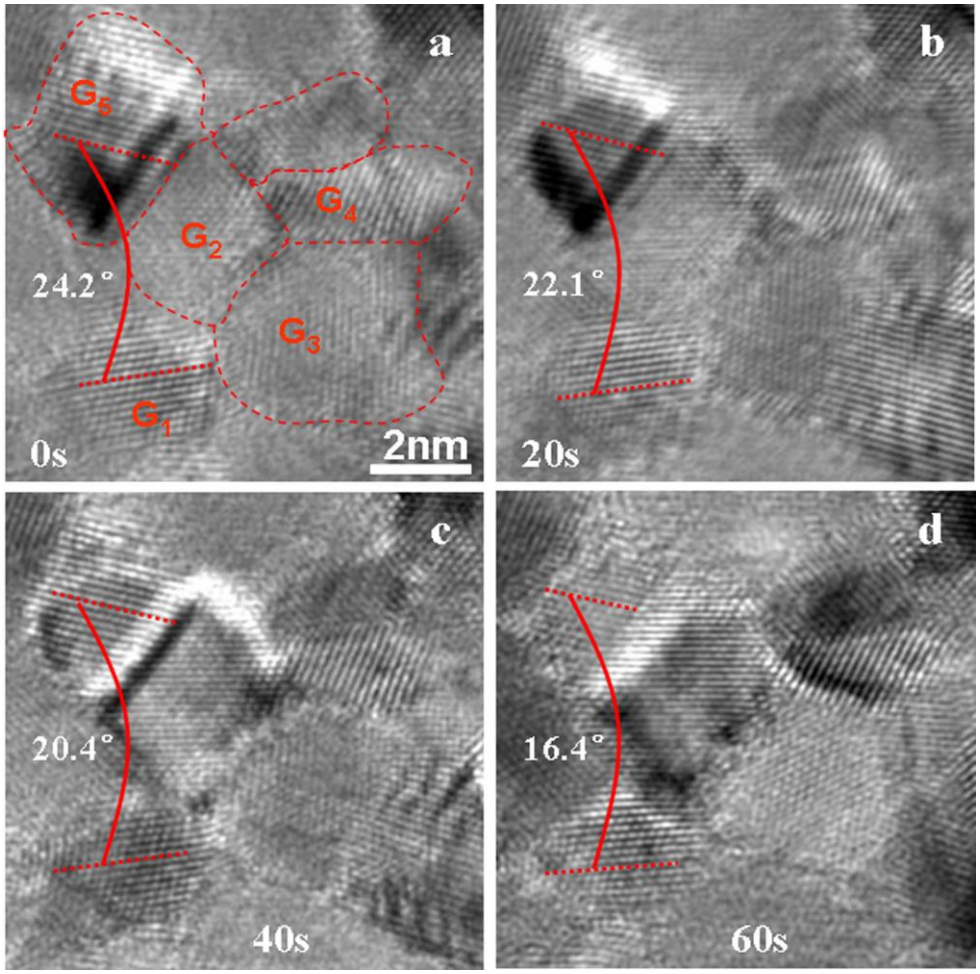

Supplementary Figure 2. Another example of the grain rotation. A series of high-resolution transmission electron microscope (HRTEM) images showing another example of the grain rotation. During the deformation, grain G_1 always exhibited obvious [110] axial-lattice, indicating that there had been no global rotation and tilting of the specimen. The G_1 was surrounded by small grains. As show in Supplementary Table 2 below, the grains undergo a collective rotation process during straining.

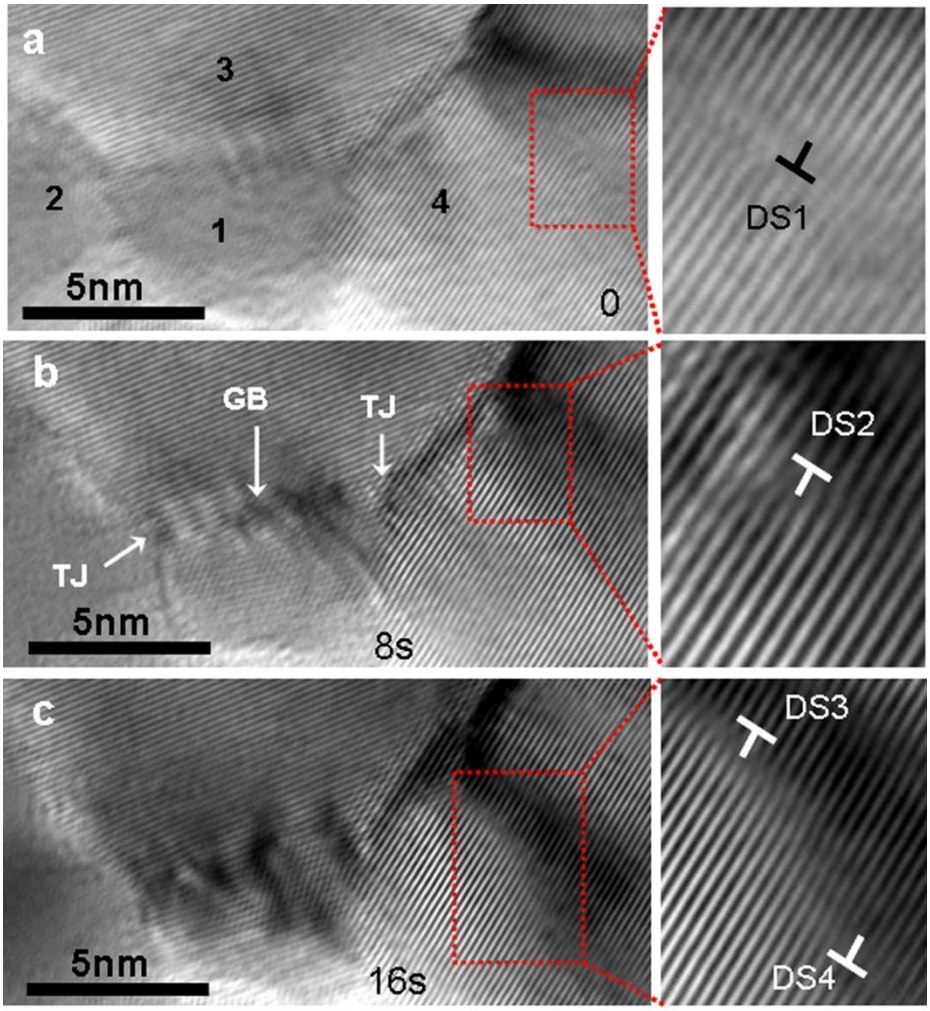

Supplementary Figure 3. Enlarged HRTEM images showing the plastic behaviors of the NC Pt. (a)-(c) HRTEM images of the same region, captured 8s apart. The small grain G_1 undergoes rotation, while full dislocations (marked with ‘‘T’’) are frequently observed in the larger grain G_4 (grain size d >10 nm). The enlarged HRTEM images taken from the red framed region of (a)-(c) clearly reveal the nucleation and motion of full dislocations in grain G_4.

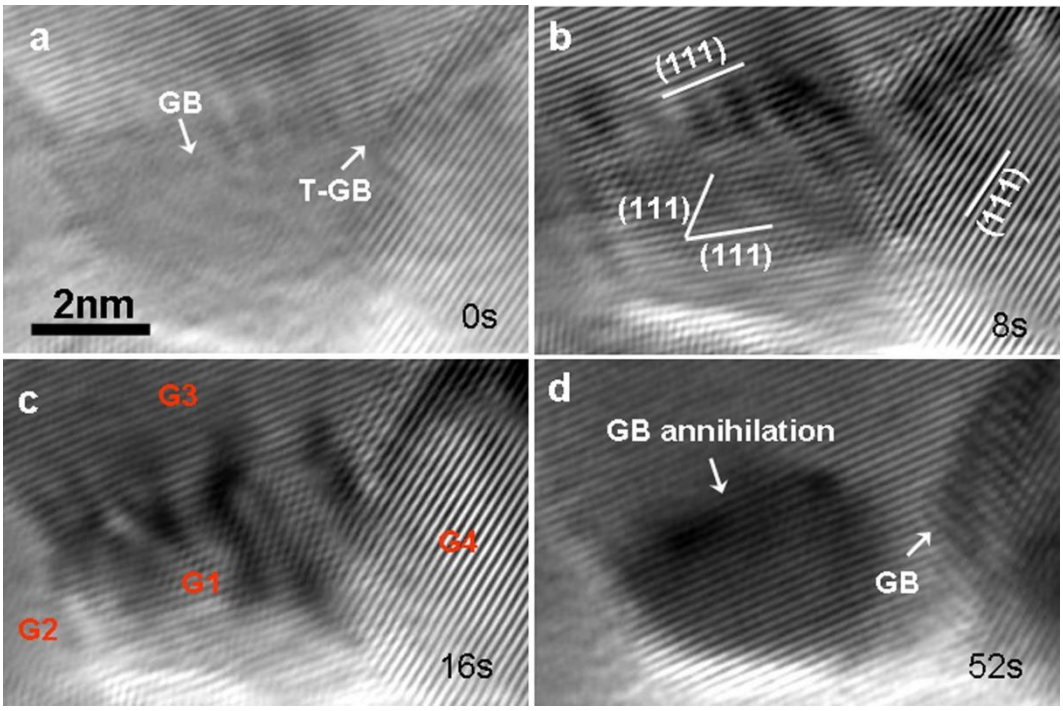

Supplementary Figure 4. Enlarged HRTEM images showing the grain boundary (GB) structure change during the grain rotation. (a) G_1 was surrounded by four high-angle GBs. (b) With further loading, G_1 exhibited obvious [110] axial-lattice, and $G_{1\text{-}2}$ and $G_{1\text{-}3}$ changed into small angle GBs. (c) With further straining, the GB angle of $G_{1\text{-}2}$ decreased and $G_{1\text{-}3}$ changed into a high-angle GB. (d) The [110] axial-lattice in G_1 changed into fringes, as the common GB disappeared and the triple junction changed into a common GB. The G_1 was surrounded by large grains, such as G_2, G_3 and G_4, only G_1 undergoes the rotation, and no rotation was observed for G_3 and G_4 (see Supplementary Table 3 below for more details).

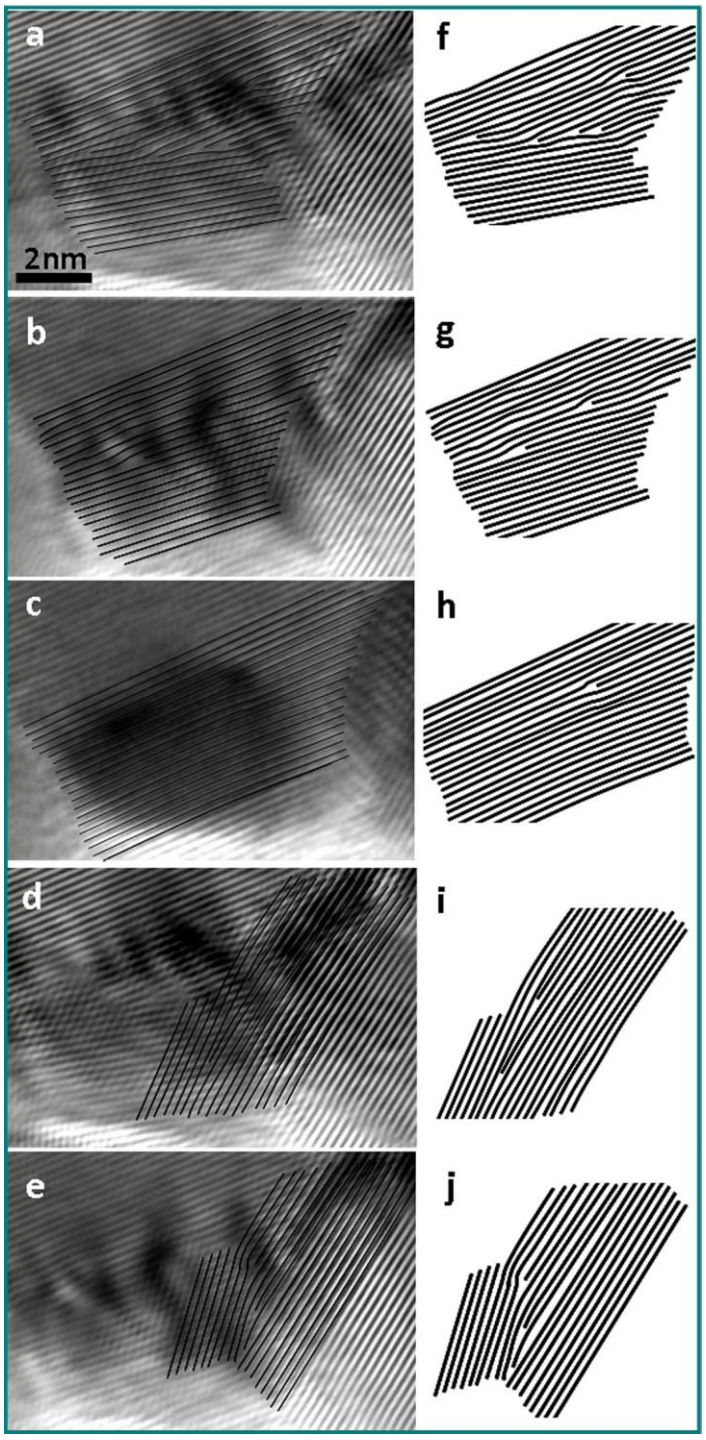

Supplementary Figure 5. *In situ* observation of the GB structure change during grain rotation. (a–c) Enlarged HRTEM images, and black lines are drawn on all of the nearly horizontal {111} planes in G_1 and G_3. (f–h) Black lines from the HRTEM images are shown separately. (d, e) Black lines are drawn on the edge-on {111} planes in G_1 and G_4 and then shown separately in (i, j).

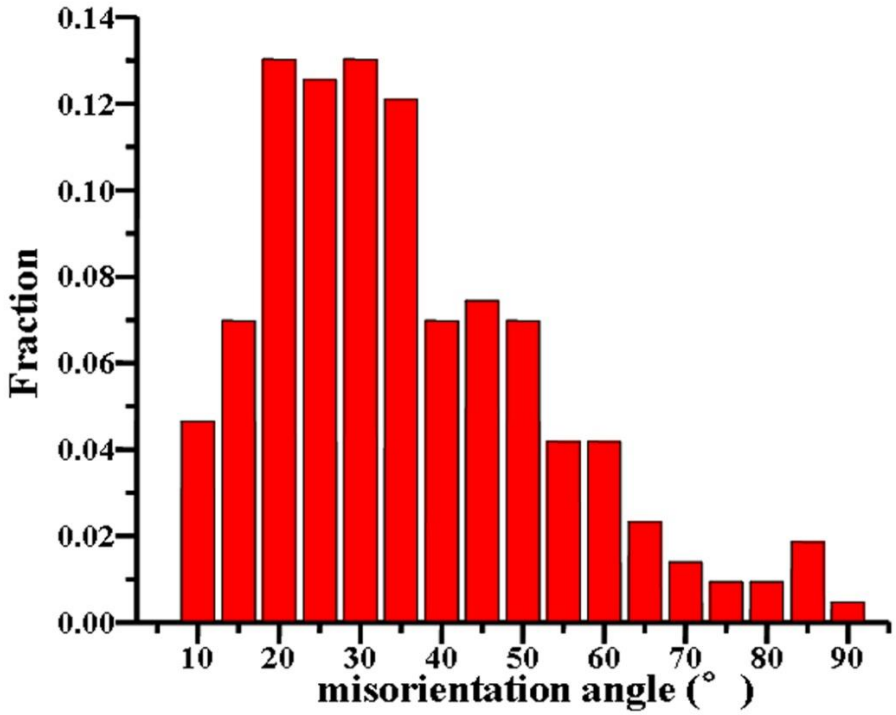

Supplementary Figure 6. The statistics of the misorientation angle distribution. The statistics of the misorientation angle distribution of the NC thin film by checking 215 nearest-neighboring grain pairs. The GBs with mis-orientation angles ranging from 8 degrees to 35 degrees are the high frequency ones (62.3%).

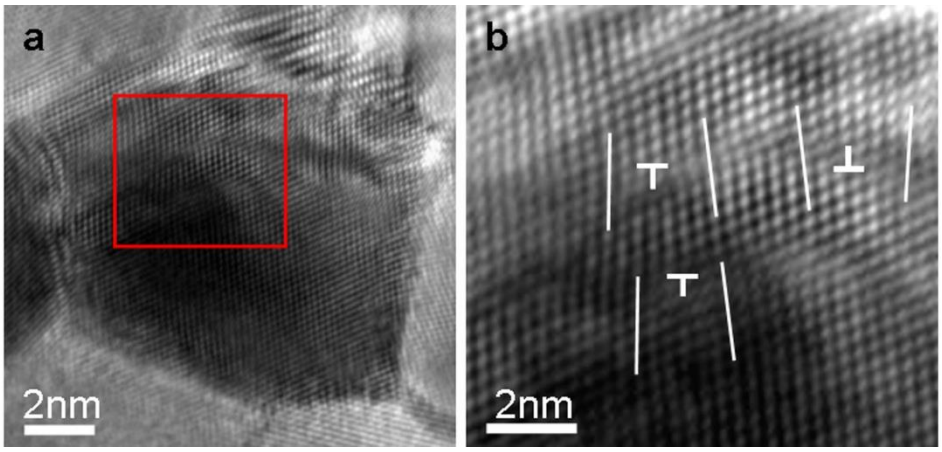

Supplementary Figure 7. Full dislocations were observed in a 14 nm sized grain after plastic deformation. (a) HRTEM image of a 14 nm-sized grain after plastic deformation. (b) Enlarged HRTEM images taken from the red framed region of (a), showing full dislocations (marked with ‘‘T’’) in the grain.

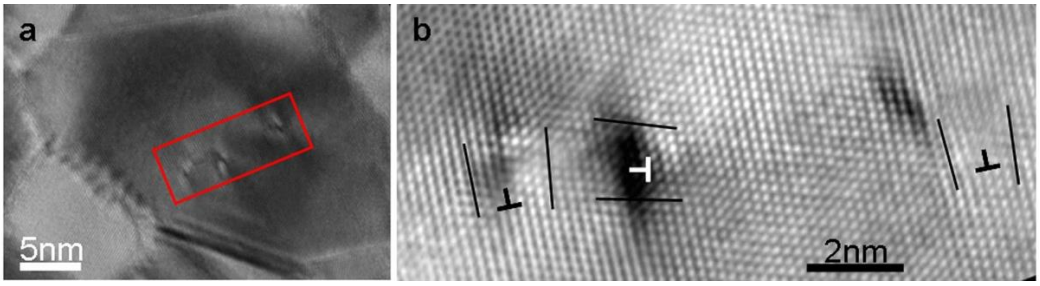

Supplementary Figure 8. Full dislocations were observed in a ~20 nm×30 nm sized grain. (b) Enlarged HRTEM images taken from the red framed region of (a), showing full dislocations (marked with ‘‘T’’) in the grain.

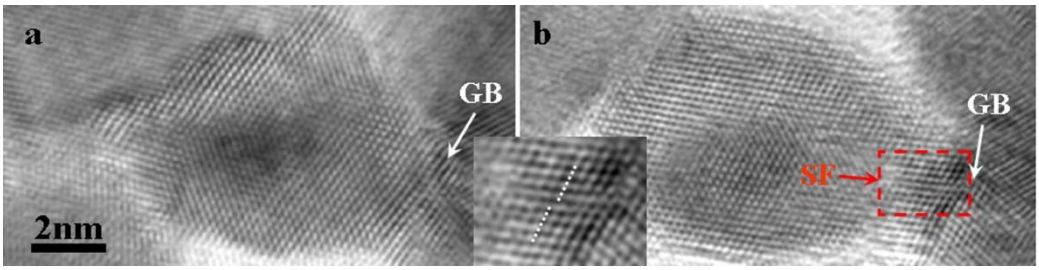

Supplementary Figure 9. **Partial dislocations were observed in a ~8 nm sized grain.** (a, b) *In situ* observation of partial dislocations (red arrow) emitted from the GB in a ~6 nm×8 nm sized grain.

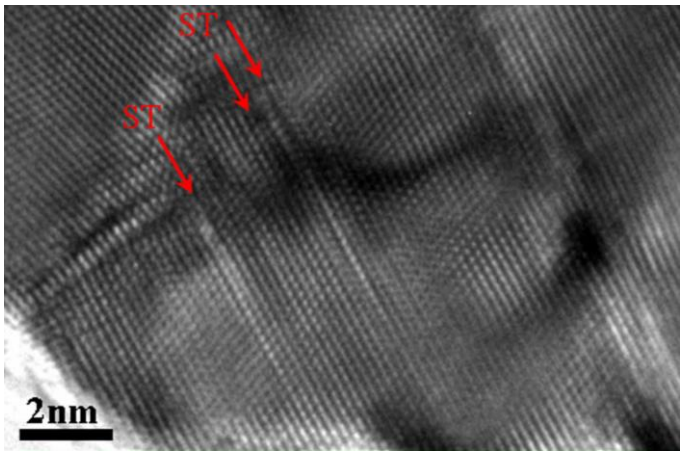

Supplementary Figure 10. Partial dislocations were observed in a ~7 nm sized grain. Other example showing the partial dislocations and resulting stacking faults (as noted by the arrows) in a ~7 nm×9 nm sized grain.

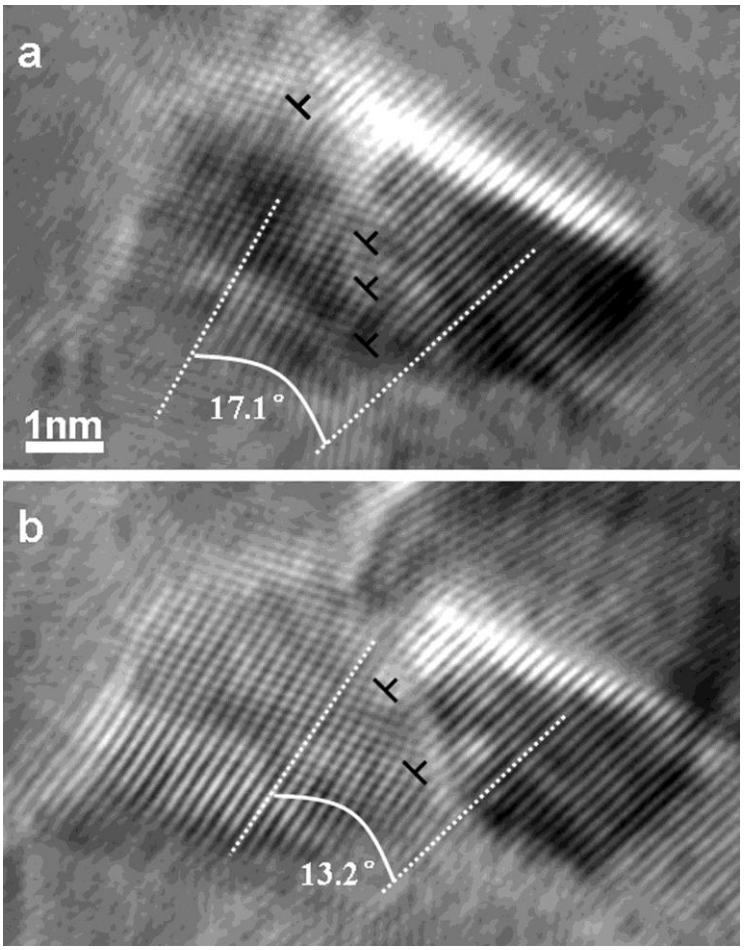

Supplementary Figure 11. Two HRTEM images taken at different points of time showing the GB dislocation mediated grain rotation process. (a) An array of dislocations (as marked with ‘‘T’’) forms a wedge-shaped disclination at the GB. (b) During straining, the number of the dislocations decreased, leading to decreasing GB angle.

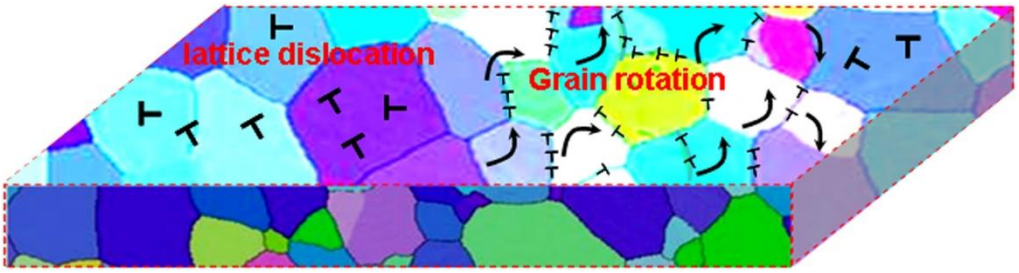

Supplementary Figure 12. Schematic illustrating the grain size effect at room temperature. Intra-grain dislocations (as marked with ‘‘T’’) dominate in larger grains and grain rotation (marked with curved arrows) via GB dislocations dominates in smaller grains.

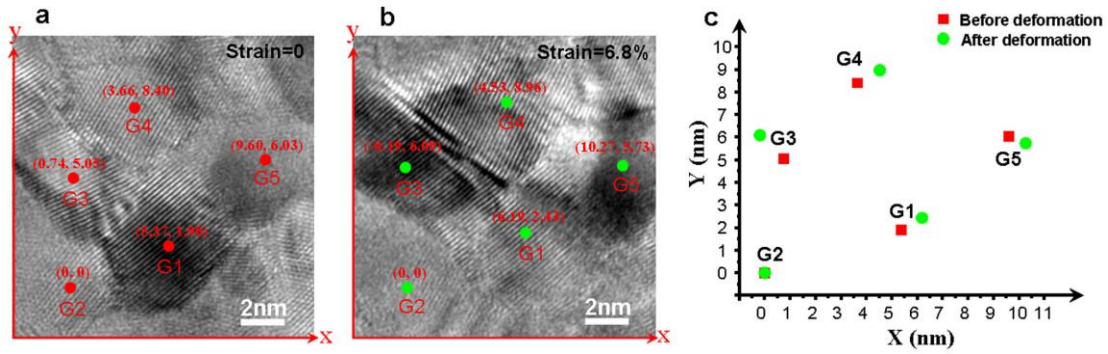

Supplementary Figure 13. **The grain switching process revealed by the grain's X-Y co-ordination evolution through the tensile processes** (a) HRTEM image corresponding to Fig. 3a in text, the position of the grains is noted as red dots; (b) HRTEM image corresponding to Fig. 3f in text, the position of the grains after grain rotation is noted as green dots. Taking the G2 as the reference grain, the position shifts of the grains can be directly measured; (c) The grains' X-Y co-ordinates before and after deformation.

Supplementary Table 1:

The rotated angles corresponding to Fig. 3 in the text. G1 was surrounded by small grains. As show in the table, G1 rotates by 9.5° with respect to G2, 13.2° with respect to G3 and 5.7° with respect to G4. We also measured the rotated angles of $G_{1\text{-}4,}$ $G_{2\text{-}3}$, $G_{2\text{-}4}$, and $G_{3\text{-}4}$: they all exhibited different values. If only one grain undergoes the rotation while the rest grains are stationary, the rotated angles of the grain with respect to others would be the same. However, the rotated angles all exhibited different values from the measurement. This indicates that all these grains rotated at the same time but to different degrees relative one another during straining.

	G1	G2	G3
G2	9.5°		
G3	13.2°	3.4°	
G4	5.7°	4°	7.6°

Supplementary Table 2:

The rotated angles corresponding to Supplementary Fig. 2. The G_1 was surrounded by small grains. As show in the table, the G_1 rotates by 0.4° with respect to G_4 and 7.8° with respect to G_5. The G_4 rotates of 8.3° with respect to G_5. The rotated angles exhibited different values; this indicates that these grains undergo a collective rotation process during straining.

	G1	G4
G4	0.4°	
G5	7.8°	8.3°

Supplementary Table 3:

The rotated angles corresponding to Fig. 4 in the text. The G_1 was surrounded by relatively large grains, such as G_2, G_3 and G_4. As show in the table, only G_1 undergoes the rotation, and no rotation was observed for the G_3 and G_4. Thus, the rotated angle of G_1 respect to G_3 and G_4 is the same, and the rotated angle of G_3 with respect to G_4 is nearly zero.

	G1	G3
G3	12.6°	
G4	12.6°	0.2 °

Supplementary Table 4:

Three examples showing the GB angle calculated from the Frank-Bilby equation in comparison with that measured during the *in situ* grain rotation experiment.

	Average spacing (nm)	Calculated angle (degree)	Measured angle (degree)
Example 1	0.90 nm	15.5°	15.2°
	1.50 nm	11.6°	11.2°
	1.60 nm	8.7°	8.5°
	2.00 nm	7.0°	7.2°
Example 2	1.05 nm	13.2°	12.5°
	2.25 nm	6.2°	4.6°
Example 3	1.95 nm	7.1°	7.5°
	1.10 nm	12.7°	15.3°
Example 4	3.10 nm	7.8°	8.3°
	1.60 nm	8.7°	10.1°
	1.17 nm	12.0°	13.5°

Supplementary Table 5:

The diffusion coefficient of FCC metals (Cu, Au and Ni…) at relatively low temperatures. D_{gb}^{C}, GB diffusion coefficient in coarse-grained metals; D_{gb}^{NC}, GB diffusion coefficient in NC metals; $D_{surface}$, surface diffusion coefficient in metals.

Diffusivity / Temperature	D_{gb}^{C} (polycrystalline)	D_{gb}^{NC} (nanocrystalline)	$D_{surface}$ (surface)
$0.25T_m$	~$3.7\times10^{-21}m^2s^{-1}$ (ref 2,3)	~10^{-19}-$10^{-18}m^2s^{-1}$ (ref 4-9)	~$8.1\times10^{-18}m^2s^{-1}$ (ref 2,3)
$0.22T_m$	~$2.6\times10^{-23}m^2s^{-1}$ (ref 2,3)	~10^{-21}-$10^{-20}m^2s^{-1}$ (ref 5-9)	~$2.5\times10^{-19}m^2s^{-1}$ (ref 2,3)

Supplementary Discussion

We now discuss why GB dislocation mediated grain rotation is observed here, in lieu of grain boundary sliding and diffusional creep. The contribution to strain rate from these latter mechanisms can be estimated as follows [1]:

For Nabarro-Herring Creep: $$\dot{e} = \frac{14\Omega s D_0 \exp(-Q/kT)}{kTd^2} \quad (1)$$

where $\dot{e}$ is the strain rate, Ω is the atomic volume, s is the stress and d is grain size, k is Boltzmann constant and T is the absolute temperature. $D=D_0 \exp(-Q/kT)$ is the lattice diffusion coefficient (the diffusion coefficient is for self-diffusion).

For Coble Creep: $$\dot{e} = \frac{14\pi\Omega s d D_{g0} \exp(-Q/kT)}{kTd^3} \quad (2)$$

Here, $D_{gb}=D_{g0}\exp(-Q/kT)$ is the GB diffusion coefficient and δ is the GB width.

For lattice diffusion controlled grain boundary sliding:

$$\dot{e} = 8\times 10^6 \frac{\mu b D_0 \exp(-Q/kT)}{kT}\left(\frac{b}{d}\right)^2\left(\frac{s}{\mu}\right)^2 \quad (3)$$

where μ is the shear modulus, b is the magnitude of the Burgers vector.

For GB diffusion controlled GB sliding:

$$\dot{e} = 2\times 10^5 \frac{\mu b D_{g0} \exp(-Q/kT)}{kT}\left(\frac{b}{d}\right)^3\left(\frac{s}{\mu}\right)^2 \quad (4)$$

Here, it should be noted that the grain boundary diffusion coefficient in NC metals (D_{gb}^{NC}) should be much higher than the data measured for coarse-grained metals (D_{gb}^{C}). For example, according to previous studies [2, 3], the calculated GB diffusion coefficient in coarse-grained FCC metals is ~3.7×10^{-21}m^{2}s^{-1} at $0.25T_m$, while the measured diffusion coefficient is ~10^{-19}m^{2}s^{-1} for NC Cu, and ~10^{-19} - 10^{-18}m^{2}s^{-1} for NC Ni [4]. When the temperature is ~300K (~$0.22T_m$), the calculated D_{gb}^{C} is ~3.3×10^{-23}m^{2}s^{-1} for Cu, while the measured D_{gb}^{NC} is ~10^{-21} - 10^{-20}m^{2}s^{-1} for the NC Cu [5-9]. This indicates that the GB diffusion coefficient in NC metals is ~ 2-3 orders

higher than the corresponding coarse-grained systems [4, 5]. See the data cited in Supplementary Table 5.

In our experiments, the temperature was below ~353 K (~0.17T_m of Pt). The GB diffusion coefficient of Pt extrapolated from bulk equation, D_{gb}^{C}, is $3.2\times10^{-28}m^2s^{-1}$ [2, 3]. Taking the GB diffusivity in NC Pt to be 3 orders of magnitude higher than that of the coarse-grained metals, the D_{gb}^{NC} of Pt is estimated to be ~ $3.2\times10^{-25}m^2s^{-1}$. Taking d=6 nm, δ=0.5 nm, σ ~0.015μ (~1 GPa) and using the equations above, the calculated strain rate is ~$1.0\times10^{-7}s^{-1}$ for diffusional creep and ~$2.4\times10^{-6}s^{-1}$ for GB sliding. The strain rate contribution from these two mechanisms is far below our experimental strain rate of ~$10^{-3}s^{-1}$.

Near the free surfaces of the thin TEM specimen, there may be some additional contribution from surface diffusion, $D_{surface}$. In the extreme case, one could use $D_{surface}$ directly. For the temperature range in question, the surface diffusion coefficient is typically one order of magnitude higher than the D_{gb}^{NC} above, based on the known data for FCC metals cited in Supplementary Table 5. As an upper bound, we take $D_{surface}$ to be two orders of magnitude higher than D_{gb}^{NC}. For our Pt foil (~10 nm in thickness), a more reasonable semi-quantitative estimate would be a combination of GB diffusion and some surface diffusion. We therefore use an average of D_{gb}^{NC} and $D_{surface}$, such that the effective diffusivity becomes ~ $3.2\times10^{-24}m^2s^{-1}$. From the equations above, the contribution to strain rate would then be ~$1.0\times10^{-6}s^{-1}$ for diffusional creep and ~$2.4\times10^{-5}s^{-1}$ for GB sliding. As we will show below, the strain rate expected from grain rotation is ~$3\times10^{-4}s^{-1}$. In other words, diffusional creep and GB sliding would at best play a secondary role when compared with grain rotation, for Pt under our experimental conditions.

In comparison, the situation would be very different for Cu and Au, because they have a much lower melting temperature (1356 K for Cu and 1336 K for Au). The GB sliding and diffusional creep can be obvious even at room temperature. For example, when the temperature is ~300 K (~0.22T_m for Cu and Au), the calculated D_{gb}^{C} is ~$3.3\times10^{-23}m^2s^{-1}$ for Cu and ~$6.1\times10^{-23}m^2s^{-1}$ for Au. Taking the GB diffusivity in NC metals to be 3 orders of magnitude higher than the coarse grained metals, the

D_{gb}^{NC} is ~$3.3\times10^{-20}m^2s^{-1}$ for Cu and ~$6.1\times10^{-20}m^2s^{-1}$ for Au, which is consistent with previous experimental measurements [5-9]. If taking d=15nm, δ=0.5nm, σ ~0.015μ for the strain rate calculation, the calculated strain rate is ~$5.1\times10^{-4}s^{-1}$ for the diffusional creep, and ~$1.1\times10^{-2}s^{-1}$ for grain boundary diffusion controlled sliding for Cu. For Au, the strain rate is ~$7.0\times10^{-3}s^{-1}$ for the diffusional creep, and ~$1.7\times10^{-2}s^{-1}$ for grain boundary diffusion controlled sliding. Most of previous experiments were carried out on such metals (Cu [6-10], Au [11], and Al [12-14]). Therefore, it is not surprising that in those cases GB sliding and diffusion creep were obviously active and observed in experiments (even when the grain size was ~15 nm [10]).

Finally, for the GB dislocation accommodated grain rotation in NC metals, the strain rate equation is [15]:

$$\dot{e} \approx f\frac{w}{t} = f\frac{2ps\,c(1-n)}{m[(1+c^2)\ln(1+c^2)-c^2\ln c^2]t} \qquad (5)$$

where f is the fraction of grains deforming via grain rotation, w is the rotation angle, v is Poisson's ratio and t is the time. Take v=0.39 and the parameter $c\approx1$ for equi-axed grains, and σ ~0.015μ, and t~60s (used in our in situ TEM observation, when the experimental observed f is about ~0.4), the calculated macroscopic strain rate due to grain rotation is ~$3\times10^{-4}s^{-1}$, which is close to the strain rate incurred in the experiments. This explains why GB dislocation mediated grain rotation is popular in the current NC Pt specimens.

Supplementary References:

1. Wang, N., Wang, Z. R., Aust, K. T. & Erb, U. Room temperature creep behavior of nanocrystalline nickel produced by an electrodeposition technique. *Mater. Sci. Eng. A* **237**, 150-158 (1997).

2. Kaur, I., Mishin, Y. & Gust, W. Fundamentals of grain and interphase boundary diffusion. (Wiley & Sons, Chichester, UK, 1995).

3. Gust, W., Mayer, S., Bögel, A., & Predel, B. Generalized representation of grain boundary self-diffusion data, *J. Physique*, **46**, C4, 537–544 (1985).

4. Würschum, R., Herth, S. & Brossmann, U. Diffusion in nanocrystalline metals and alloys - A status report. *Adv. Eng. Mater.* **5**, 365–372 (2003).

5. Christian, H. & Sergiy, V. D. Grain boundary diffusion in metals: recent developments. *Material Transactions* **44,** 14-27 (2003).

6. Chokshi, A. H., Rosen, A., Karch, J. & Gleiter, H. On the validity of the Hall-Petch relationship in nanocrystalline materials. *Scripta Mater.* **23**, 1679–1684 (1989).

7. Horváth, J., Birringer, R., & Gleiter, H. Diffusion in nanocrystalline material. *Solid State Comm.* **62**, 319-322 (1987).

8. Cai, B., Kong, Q. P., Lu, L. & Lu, K. Low temperature creep of nanocrystalline pure copper. *Mater. Sci. Eng. A* **286**, 188–192 (2000).

9. Masumura, R. A., Hazzledine, P. M. & Pande, C. S. Yield stress of fine grained materials. *Acta. Mater.* **46,** 4527-4534 (1998).

10. Meyers, M. A., Mishra, A. & Benson, D. J. Mechanical properties of nanocrystalline materials. *Prog. Mater. Sci.* **51**, 427–556 (2006).

11. Olliges, S., Frank, S., Gruber, P. A., Auzelyte, V., Solak, H. & Spolenak, R. Thermo mechanical properties and plastic deformation of gold nanolines and gold thin films. *Mater. Sci. Eng. A* **528**, 6203–6209 (2011).

12. Rupert, T. J., Gianola, D. S., Gan, Y. & Hemker, K. J. Experimental observations of stress-driven grain boundary migration. *Science* **326**, 1686-1689 (2009).

13. Jin, M., Minor, A. M., Stach, E. A. & Morris, J. W. In situ TEM observations of fast grain-boundary motion in stressed nanocrystalline aluminum films. *Acta Mater.* **52**, 5381-5387 (2004).

14. Legros, M., Gianola, D. S. & Hemker, K. J. In situ TEM observations of fast grain-boundary motion in stressed nanocrystalline aluminum films. A*cta Mater.* **56**, 3380-3393 (2008).

15. Ovid'ko, I. A. & Sheinerman, A. G. Special rotational deformation in nanocrystalline metals and ceramics. *Scripta Mater*. **59,** 119-122 (2008).